[16]H. F. Berg (private communication).
[17]J. R. Greig and G. Palumbo, Phys. Fluids 12, 1211 (1969).
[18]T. N. Lie, M. J. Rhee, and E. A. McLean, Phys. Fluids 13, 2492 (1970).
[19]J. Cooper and J. R. Greig, J. Sci. Instr. 40, 433 (1963).
[20]J. R. Greig and J. Cooper, Appl. Opt. 7, 2166 (1968).
[21]W. W. Jones and J. R. Greig, University of Maryland Technical Report No. 943, 1969 (unpublished).
[22]R. Chabbal, J. Rech. Centre Natl. Rech. Sci. Lab. Bellevue (Paris) 24, 1386 (1953); we used an English translation by R. B. Jacobi, U.K.A.E.A., Harwell, England.
[23]J. R. Greig, dissertation (University of London, 1965) (unpublished).
[24]D. J. Bradley, J. Sci. Instr. 39, 41 (1962).
[25]W. W. Jones, H. R. Griem, J. R. Greig, and M. H. Miller, Bull. Am. Phys. Soc. 15, 1513 (1970).
[26]H. P. Larson and K. L. Andrew, Appl. Opt. 6, 170 (1967).
[27]H. Cramer, *Mathematical Methods of Statistics* (Princeton U. P., Princeton, N. J., 1966), p. 191.
[28]G. Hammond, dissertation (University of Maryland, 1971) (unpublished).
[29]M. Yamamoto, Phys. Rev. 146, 137 (1966).
[30]J. Roberts and K. R. Eckerle, Phys. Rev. 159, 104 (1967).
[31]J. S. Hildum and J. Cooper, Phys. Letters 36A, 153 (1971).
[32]P. Burke and D. Moores U.K.A.E.A. Report No. HL. 68/5695, Harwell, 1968 (unpublished).
[33]K. S. Barnes, J. Phys. B 4, 1377 (1971).
[34]H. R. Griem, Phys. Rev. 165, 258 (1968).

PHYSICAL REVIEW A VOLUME 5, NUMBER 6 JUNE 1972

Calculated Bremsstrahlung Spectra from Thick Tungsten Targets*

Ellery Storm
Los Alamos Scientific Laboratory, Los Alamos, New Mexico 87544
(Received 3 September 1971)

The bremsstrahlung energy distribution from a thick tungsten target is calculated from the Sommerfeld and Born-approximation thin-target formulas, taking into account electron energy losses, electron backscatter losses, and photon attenuation in the target. Over-all agreement with measurement is 20% in the 12–100-keV energy range, increasing to 50% at 300 keV. Semiempirical expressions are developed that give 20% over-all agreement with measurement in the 12–300-keV energy range.

I. INTRODUCTION

The x-ray spectrum produced by low-energy electrons striking a target is not only interesting theoretically but also because x rays are used extensively in medicine and industry. Ehrlich[1] compared thick-target bremsstrahlung theory to her measurements and found "order-of-magnitude agreement." Recently, absolute measurements by Unsworth and Greening[2] in the 15–30-keV energy range and by Storm, Israel, and Lier[3] in the 12–300-keV energy range have been reported. Previous measurements below 300 keV include those of Hettinger and Starfelt,[4] Dyson,[5] and Placious.[6] Sufficient experimental information is now available to permit a reevaluation of the thick-target bremsstrahlung theory.

The semiclassical formula of Kramers[7] has been used extensively to calculate thick-target spectra, although it neglects electron backscatter and photon attenuation losses. Unsworth and Greening[2] obtained agreement with their measurements by correcting the Kramers formula for photon attenuation.

Berger and Seltzer[8–10] have developed a Monte Carlo program for calculating bremsstrahlung spectra which includes electron and photon multiple scattering. Their calculations for normal incidence of the electron beam on the target are in good agreement with the measurements of Placious.[6] In the present calculation, thin-target bremsstrahlung formulas developed from quantum mechanics are corrected for electron energy losses, electron backscatter losses, and photon attenuation to obtain thick-target bremsstrahlung distributions that can be compared to measurement. Semiempirical equations also are compared to measurement, and one is developed that gives 20% agreement below 300 keV.

II. THIN-TARGET BREMSSTRAHLUNG FORMULAS

Bremsstrahlung cross-section theory has been developed either with Sommerfeld-Maue wave functions or in the plane-wave Born approximation. The thin-target bremsstrahlung formulas have been reviewed by Koch and Motz.[11] Of the formulas differential in photon energy, the Sommerfeld formula[12] and the formulas labeled 3BN and 3BN(a) by Koch and Motz are applicable below 300 keV. In

the Koch and Motz notation, the number 3 indicates that the formula is differential with respect to photon energy. The first letter will be either B for Born approximation or S for Sommerfeld, and the second letter N indicates no screening.

Recently bremsstrahlung cross-section calculations have been made by Brysk, Zerby, and Penny,[13] Elwert and Haug,[14] and Tseng and Pratt[15] based on partial wave expansions numerically evaluated using the Dirac equation and a screened Coulomb potential. For a high-atomic-number element, $z=79$, these authors have calculated bremsstrahlung cross sections in the energy region of interest here (less than 300 keV) for the following initial electron energies (E_0) and photon energies (k). Tseng and Pratt[15] give cross sections integrated over electron direction alone as a function of photon angle and the total cross section integrated over both electron and photon direction for $E_0=50$ keV, $k=20$ and 30 keV; $E_0=128$ keV, $k=96$ keV; and $E_0=180$ keV, $k=108$ keV. Elwert and Haug[14] give cross sections integrated over electron direction alone as a function of photon angle for $E_0=180$ keV, and cross sections integrated over both electron and photon direction as a function of photon energy for $E_0=45$ keV. Brysk, Zerby, and Penny[13] give cross sections integrated over electron direction as a function of photon angle for $E_0=180$ keV and $k=108$ keV. In addition, Rester, Edmonson, and Peasley[16] compare their experimental cross sections to theoretical cross sections integrated over electron direction alone as a function of photon angle which were obtained from a modification of the Brysk *et al.* computer program for $E_0=50$ keV, $k=10$, 20, 30, and 40 keV; and $E_0=200$ keV, $k=80$, 120, and 160 keV.

Sommerfeld obtained the cross section for a photon emitted in a given direction with a fixed electron recoil energy. Kirkpatrick and Wiedmann[17] calculated the cross section integrated over the emission directions of the electrons and photon. The Sommerfeld-Kirkpatrick-Wiedmann cross section (3SN) is nonrelativistic and neglects screening and retardation effects. Of the Born-approximation formulas, Koch and Motz recommend the nonscreened nonrelativistic formula of Heitler,[18] 3BN(a), for the 10–100-keV energy range, and the nonscreened relativistic formula of Bethe and Heitler,[19] Sauter,[20] and Gluckstern and Hull,[21] 3BN, for the 100–300-keV energy range. They recommend further that both formulas be multiplied by the Elwert[22] Coulomb correction factor, and that formula 3BN be multiplied by an empirical correction factor A which varies with the initial electron energy.

Thin target bremsstrahlung energy distributions computed from these formulas are shown in Fig. 1 for $Z=74$ and initial electron energies of 12, 30, 60, 100, 200, and 300 keV. The distributions are given as a function of photon energy k and are in units of erg/mA sec keV sr (g/cm^2) of target area. The Born-approximation formulas include the Elwert factor, but not the empirical correction.

The 3SN distributions fall off less rapidly with photon energy than do the Born-approximation distributions, and although nonrelativistic 3SN predicts more energy at higher photon energies than the relativistic 3BN formula. The nonrelativistic 3BN(a) formula predicts less energy than the relativistic 3BN formula and the discrepancy increases with initial electron energy. For example, the 3BN(a) values are low by only 3–5% at 12 keV, but differ by 20–30% at 100 keV and by more than a factor of 2 at 300 keV. Because 3BN differs from 3BN(a) by only a few percent at the lower energies and is expected to be more accurate at the higher energies where relativistic effects are important, formula 3BN(a) will not be considered further.

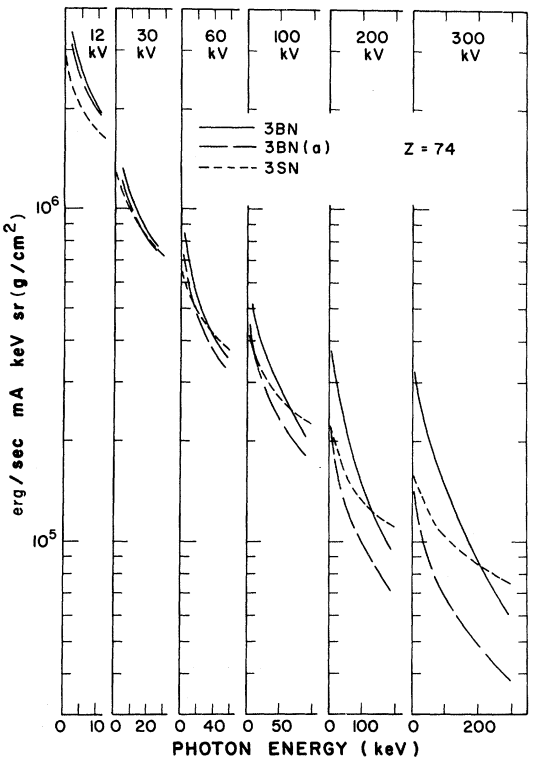

FIG. 1. Thin-target bremsstrahlung energy distribution as a function of photon energy for several initial electron energies. The distributions were calculated by using the nonrelativistic Sommerfeld-Kirkpatrick-Wiedmann 3SN formula, and the nonrelativistic 3BN(a) and relativistic 3BN Born-approximation formulas. The Elwert Coulomb correction is included in the Born-approximation formulas.

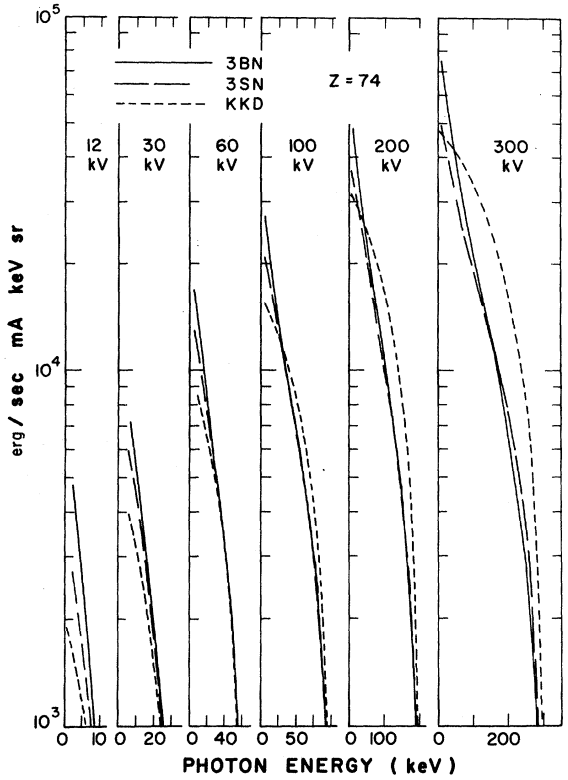

FIG. 2. Thick-target bremsstrahlung energy distribution as a function of photon energy for several initial electron energies. The distributions were calculated from the thin-target bremsstrahlung formulas 3SN and 3BN with only the electron energy loss by collisions with atomic electrons included. Also shown is the energy distribution calculated from the semiempirical KKD formula.

III. THICK-TARGET BREMSSTRAHLUNG FORMULAS

A. Electron Energy Loss

A thick-target distribution can be obtained from the thin-target distribution by calculating the electron energy loss with target depth by collisions with atomic electrons. The target is divided into a number of thin strips in each of which there is an energy loss ΔE, which is selected by assuming a continuous slowing down approximation. If E_0 is the initial electron energy, E is the electron energy at photon emission, and $I_{E_0,k,E}$ is the thin-target bremsstrahlung emission per path length per unit solid angle in the photon energy interval k to $(k+dk)$, then the thick-target emission $I_{E_0,k}$ is given by

$$I_{E_0,k}=\int_{E>k}^{E_0} I_{E_0,k,E}\left(\frac{dE}{-dE/dx}\right), \qquad (1)$$

where dE/dx, the mean electron energy loss per unit path length, has been tabulated by Berger and Seltzer[23] for tungsten using Bethe's stopping-power theory. If $I_{E_0,k,E}$ is in units of erg/sec mA keV sr (g/cm^2), then dE/dx is in keV cm^2/g and dE in keV. The thick-target energy distributions calculated from Eq. (1) by numerical integration are shown in Fig. 2 as a function of photon energy k for the same values of E_0 given in Fig. 1. $I_{E_0,k}$ is in units of erg/sec mA keV sr and has been calculated by using both 3SN and 3BN formulas for $I_{E_0,k,E}$.

The thick-target distributions computed from Eq. (1) are comparable to the distributions calculated from the Kramers[7] semiclassical nonrelativistic formula. Kramers started with the classical expression for the spectral distribution of the energy radiated by an electron moving in the Coulomb field of an atom, applied the correspondence principle to assume that quantum energy was equal to the classical energy of the emitted radiation, and neglected all energies above E_0. After obtaining the thin-target distribution, he used the Thomas-Whiddington law to calculate the electron energy loss with target depth, and obtained a thick-target distribution that agreed with an empirical equation obtained earlier by Kulenkampff.[24] Dyson[5] evaluated the constant in the equation which may be written in the form

$$I_{E_0,k}=(27.6/4\pi)Z(E_0-k) \quad (\text{ergs/sec mA keV sr}) . \qquad (2)$$

The distribution calculated from the Kramers-Kulenkampff-Dyson (KKD) formula is compared (Fig. 2) to the distribution obtained from Eq. (1) by using the 3SN and 3BN thin-target formulas. The KKD formula is in reasonable agreement with Eq. (1) although it tends to predict larger bremsstrahlung emission than either 3SN or 3BN at the higher photon and initial electron energies.

B. Electron Backscatter Loss

Equations (1) and (2) do not include electron backscattering losses and photon attenuation in the target. Electron backscattering losses may be included in Eq. (1) by writing

$$I_{E_0,k}=\int_{E>k}^{E_0} I_{E_0,k,E}\left(\frac{dE}{-dE/dx}\right)(1-\eta\epsilon_{E_0,k,E}) . \qquad (3)$$

The fraction of the incident electrons backscattered from a thick target η is nearly independent of E_0 and has a value of 0.5 for tungsten.[25,26] Because any electron backscattered with an energy less than E_0 has contributed to the ionization, η is multiplied by $\epsilon_{E_0,k,E}$, the fraction of the total number of electrons averaged over all angles backscattered with energies between E and E_0. The fraction $\epsilon_{E_0,k,E}$ was obtained by graphical integration of the average electron backscatter distribution measurements,[27-30] where the angles of incidence of the electron beam were in the range 0–45°, which is similar to the angles of incidence considered here.

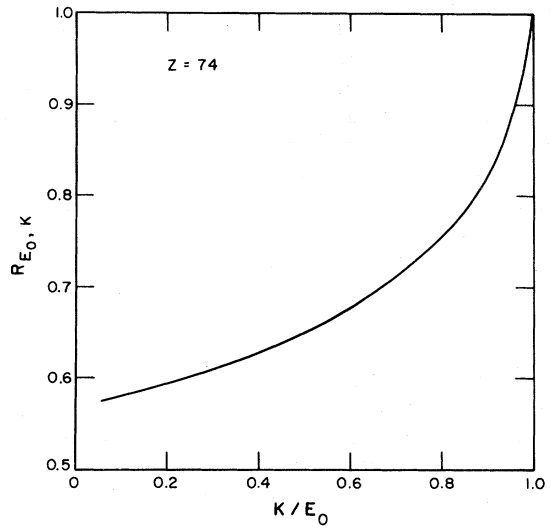

FIG. 3. Electron backscatter loss correction as a function of the ratio of the photon energy k to the initial electron energy E_0.

An estimate of the backscatter correction can be obtained from the ratio

$$R_{E_0,k}=\int_{E>k}^{E_0} I_{E_0,k,E}\left(\frac{dE}{-dE/dx}\right)(1-\eta\epsilon_{E_0,k,E})\Big/$$

$$\int_{E>k}^{E_0} I_{E_0,k,E}\left(\frac{dE}{-dE/dx}\right). \quad (4)$$

Figure 3 gives $R_{E_0,k}$ as a function of the ratio of the photon energy to the initial electron energy.

C. Photon Attenuation

An exponential term can be applied to the integrand of Eq. (3) to correct for photon attenuation:

$$I_{E_0,k}=\int_{E>k}^{E_0} I_{E_0,k,E}\left(\frac{dE}{-dE/dx}\right)\times(1-\eta\epsilon_{E_0,k,E})\,e^{-\mu_k x/\tan\alpha}. \quad (5)$$

The geometry assumed in Eq. (5) is shown in Fig. 4 and is typical of the geometry used in the measurement of x-ray spectra. The angle between the incident electron beam and the normal to the target is defined as the target angle α. The photons reflected from the target are observed 90° to the electron beam. Thus, the photons are attenuated by a target thickness $x/\tan\alpha$, where x is the distance the electron penetrates before photon emission. The total attenuation coefficient[31] of a photon with energy k is μ_k.

An estimate of the photon attenuation correction can be obtained from the ratio

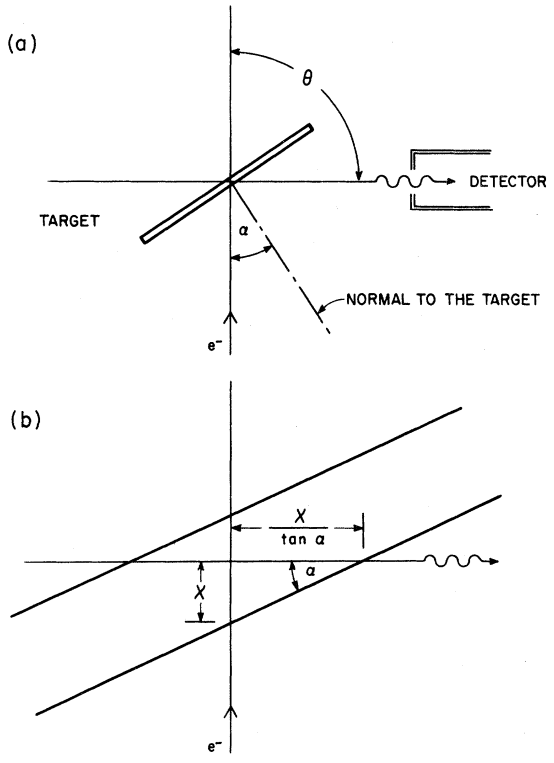

FIG. 4. Sketches showing the geometry assumed in the calculation of the photon attenuation in the target.

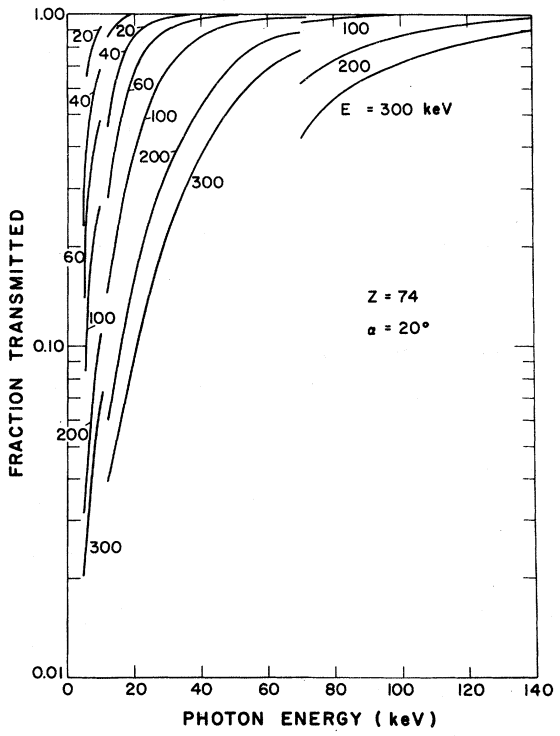

FIG. 5. Photon attenuation correction factor as a function of photon energy for several values of E_0 and a target angle of 20°.

TABLE I. Partial summary of absolute measurements of x-ray spectra.

Authors	X-ray unit	X-ray tube	Wave form	Inherent filtration	Target material	Target angle (deg)	Tube potential (keV)	Tube current	Detector	Detection angle (deg)
Ehrlich (Ref. 1)	···	experimental	constant potential	0.272 g/cm^2 Be	tungsten	22	50, 100	0.01 μA	NaI	90
Dyson (Ref. 5)	···	projection microscopy	constant potential	none	gold	0	12	0.05–0.1 μA	proportional counter (Ar)	0
Hettinger and Starfelt (Ref. 4)	Siemens Heliophos-Tutomat	Rotalix	full wave rectified	~0.7 mm Al	tungsten	?	45, 75	0.6–0.8 mA	NaI	90
	Phillips	MG-300	constant potential	~4 mm Al	tungsten	22	100, 140, 170, 220, 250	0.1–0.6 mA	NaI	90
Placious (Ref. 6)	N.B.S. 500-keV accelerator	electron	constant potential	0.02 in. Be	gold (18.7 mg/cm^2 thick)	60	50, 100	?	NaI	110
Rester, Dance, and Derrickson (Ref. 32)	Van de Graaff accelerator		constant potential	0.005 in. Mylar	gold	0	200	?	NaI	120
Unsworth and Greening (Ref. 2)	···	Machlett OEG-50	constant potential	0.001 in. Be	tungsten	20	15, 20 25, 30	?	NaI and proportional counter (Ar)	90
Storm, Israel, and Lier (Ref. 3)	Norelco	Müller Mö 301/10	constant potential	0.71 g/cm^2 Araldit plastic 0.65 g/cm^2 Pyrex glass 0.44 g/cm^2 Be 1.4 g/cm^2 oil	tungsten	22.5	100, 150, 200, 250, 300	2 mA	Si and Ge semiconductors, NaI, and Xe proportional counter	90
	Triplett-Barton	Machlett EG-252-C	self-rectified	0.425 g/cm^2 Be	tungsten	20	60, 80, 100, 150, 200	1 mA	Si and Ge semiconductors NaI, and Xe proportional counter	90
	100-kV Picker	Machlett MR-100	self-rectified	0.28 g/cm^2 Pyrex glass	tungsten	20	40, 60, 80, 100	2 mA	Si and Ge semiconductors, NaI, and Xe proportional counter	90
	60-kV Picker	Machlett OEG-60G	constant potential	0.046 g/cm^2 Be	tungsten	45	12, 20 40, 60	2 mA	Si and Ge semiconductors, NaI, and Xe proportional counter	90

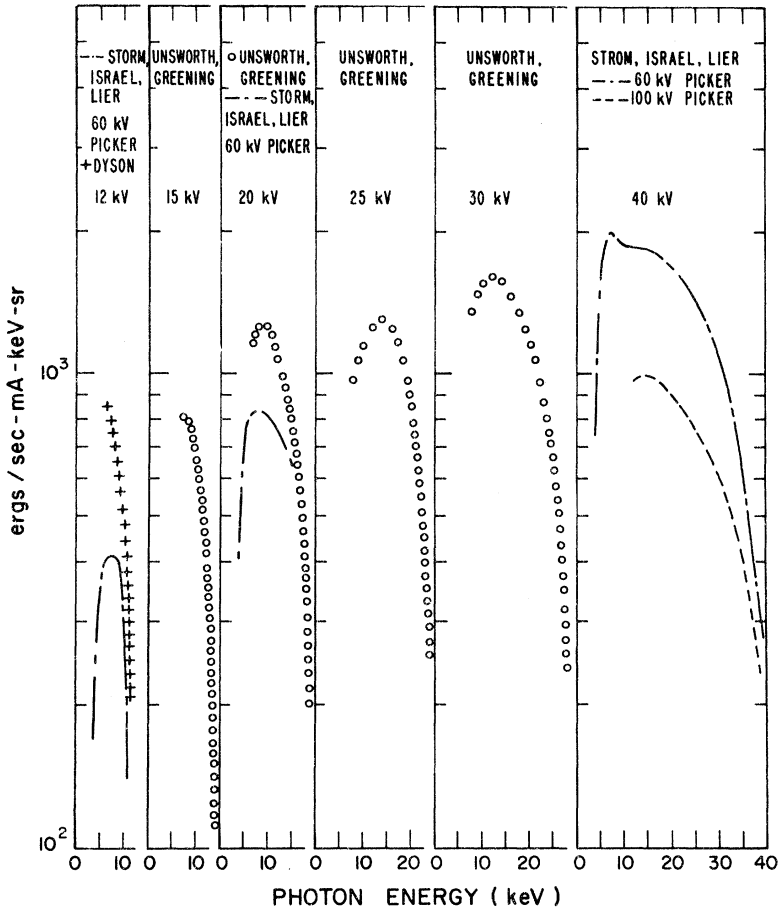

FIG. 6. Measured x-ray spectra. Experimental conditions are given in Table I.

$$f_{E_0,k,\alpha}=\int_{E>k}^{E_0} I_{E_0,k,E}\left(\frac{dE}{-dE/dx}\right)(1-\eta\epsilon_{E/E_0,u_0}) \times e^{-\mu_k x/\tan\alpha}\Big/\int_{E>k}^{E_0} I_{E_0,k,E}\left(\frac{dE}{-dE/dx}\right)(1-\eta\epsilon_{E/E_0,u_0}) \cdot \tag{6}$$

Typical values of $f_{E_0,k,\alpha}$ are plotted in Fig. 5 as a function of photon energy for several values of E_0 and a target angle of 20°. Within 3%, the same values of $f_{E_0,k,\alpha}$ are obtained with either formula 3SN or 3BN in Eq. (6).

D. Comparison with Measurement

A direct comparison of experimental x-ray spectra is complicated by differences in excitation potential, wave form, inherent filtration, target material, target angle, and detector angle. Table I gives a partial summary of the various parameters employed by different investigators. Figures 6–9 show many of the absolute measurements of x-ray spectra for high-Z target materials in the energy range 12–300 keV. Only corrections for inherent filtration and conversions from photons to ergs have been applied to the reported data.

Calculated thick-target bremsstrahlung energy distributions, with electron backscatter and photon attenuation included, are compared (Fig. 10) to some typical measurements made at initial electron energies, or accelerating potentials, of 12, 30, 60, 100, 200, and 300 kV. The distributions labeled 3SN and 3BN were calculated by using the thin target 3SN and 3BN formulas for $I_{E_0,k,E}$ in Eq. (5). The distribution labeled KKD was calculated from Eq. (2) with corrections for backscatter given by Eq. (4), and photon attenuation given by Eq. (6). The agreement is good at the lower potentials, but at the higher potentials the 3SN and 3BN distributions tend to lie below the measurements and the KKD distribution lies above the measurements.

These trends are seen more clearly in Fig. 11, where the average and extreme measured-to-calculated ratios are plotted as a function of accelerating potential. Many measurements made with constant-potential accelerators operating in the 12–300-keV energy range with high-Z targets are included. In these measurements where the inher-

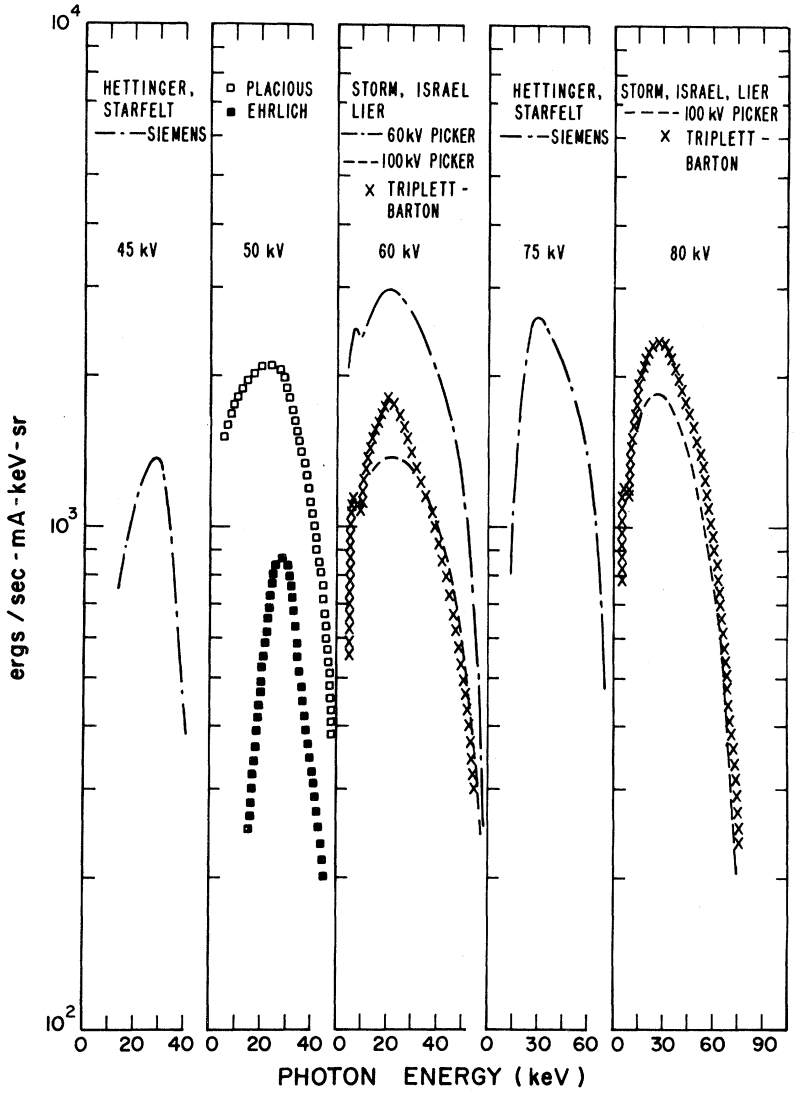

FIG. 7. Measured x-ray spectra. Experimental conditions are given in Table I.

ent filtration corrections were large, the lower portion of the spectrum was not included in the ratio calculations. When the target was not tungsten or the geometry was different than that indicated in Fig. 4, appropriate Z and angular corrections were applied. For example, Dyson[5] measured the photons transmitted through a gold target, and Placious[6] used a gold target at a 60° target angle with an observation angle of 110°. The ratios indicate that the KKD calculation gives the best fit to the measured spectral shape at the lower potentials. However, at the higher potentials and photon energies, the KKD calculation predicts larger emission rates than are measured and gives the poorest fit to the spectral shape. The 3SN calculation predicts smaller emission rates at the lower photon energies than does the 3BN calculation, but a study of the ratios indicates that there is no basis for preferring one calculation rather than the other. With two or three exceptions, the average ratios indicate that both 3SN and 3BN give 20% agreement below 100 keV. Above 100 keV, the ratios tend to increase progressively, reaching 40–50% at 300 keV.

As mentioned earlier, Koch and Motz[11] suggest that an empirical factor A be applied to formula 3BN. In Fig. 23 of Ref. 11, values of A for $Z = 13$ and 79 and energies above 100 keV are given. Values for A interpolated for $Z = 74$ are given in Fig. 11 together with a least-square fit through the average 3SN and 3BN ratios. If either A or the least-square values are used as an empirical multiplicative correction to Eq. (5), 20% agreement with measurement is obtained over the 12–300-

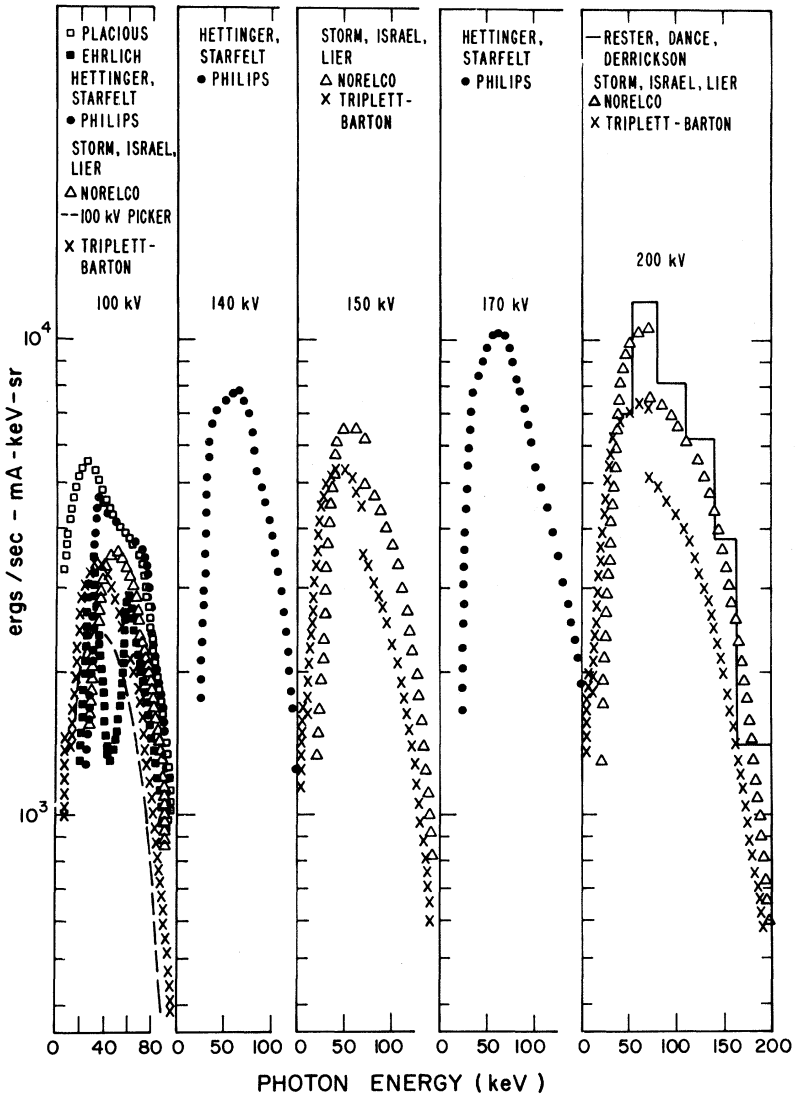

FIG. 8. Measured x-ray spectra. Experimental conditions are given in Table I.

keV energy range.

IV. SEMIEMPIRICAL THICK-TARGET BREMSSTRAHLUNG FORMULAS

The semiempirical KKD formula [Eq. (2)] has been used extensively to calculate thick-target spectra. Figure 12 compares Eq. (2) to measurement and shows satisfactory agreement at the lowest potentials, but the agreement becomes increasingly poor as the potential increases. Figure 10 shows that agreement is improved when backscatter and photon attenuation corrections are included in Eq. (2).

Better agreement with measurement is obtained with an expression of the form

$$I_{E_0,k} \approx \left(\frac{21}{4\pi} Z \frac{E_0 - k}{(k/E_K)^{1/3}}\right) R_{E_0,k} f_{E_0,k,\alpha} \left(\frac{\text{erg}}{\text{sec mA keV sr}}\right), \quad (7)$$

where E_K is the ionization potential of the K shell (69.5 keV for tungsten), and E_0, k, and E_K are in keV. The term in large parentheses in Eq. (7) is a modification of the KKD formula that approximates Eq. (1) with formula 3BN used to represent the thin-target distribution. The electron backscatter $R_{E_0,k}$ and photon attenuation $f_{E_0,k,\alpha}$ corrections are given by Eqs. (4) and (6). Equation (7) is compared to measurement in Fig. 12, and the overall agreement is within 20% up to accelerating potentials of 200 kV.

As Fig. 12 shows, still better agreement is obtained with the following expression:

$$I_{E_0,k} \approx \left(\frac{11}{4\pi} Z \frac{(E_0 - k)(1 - e^{-3k/E_K})}{(k/E_0)^{1/3}(1 - e^{-E_0/E_K})}\right) f_{E_0,k,\alpha}$$

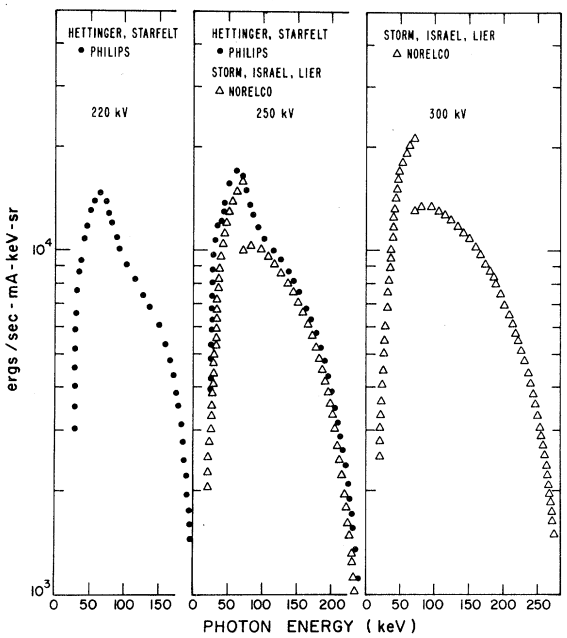

FIG. 9. Measured x-ray spectra. Experimental condition are given in Table I.

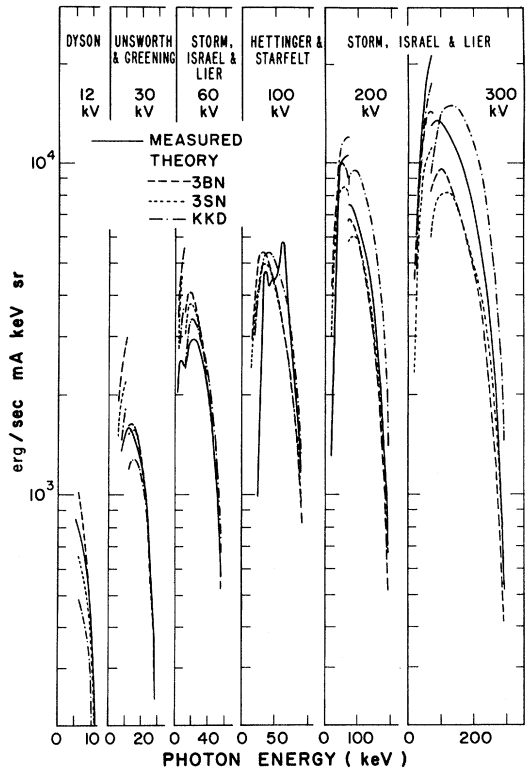

FIG. 10. Comparison of measured and calculated thick-target bremsstrahlung energy distributions plotted as a function of photon energy for several accelerating potentials. The calculated distributions shown in Fig. 2 have been corrected for electron backscatter losses and photon attenuation in the target. For clarity, the L-edge structure (10–12 keV) has been omitted.

$$\left(\frac{\text{ergs}}{\text{sec mA keV sr}}\right), \qquad (8)$$

where the term in the large parentheses is an approximation to Eq. (3), and the thin-target formula 3BN is corrected for both electron energy and backscatter loss. Equation (8) gives 20% agreement up to accelerating potentials of 300 kV.

For photon energies $k > E_{L_I}$, the ionization potential of the L_I shell (12 keV for tungsten), the photon attenuation correction can be approximated by

$$f_{E_0,k,\alpha} \approx \exp(-0.2 C_{E_0,k} \Re_{E_0} \mu_k / \tan\alpha), \qquad (9)$$

where $\Re_{E_0}$ is the range of an electron with inital energy E_0, and $C_{E_0,k}$ is a dimensionless correction as shown in Fig. 13.

V. CONCLUSIONS

The thin-target bremsstrahlung formulas 3BN and 3SN are differential with respect to the photon energy and are obtained by integrating over the emission directions of the electron and photon. Therefore, the energy distribution represents an average over the direction of photon emission. In

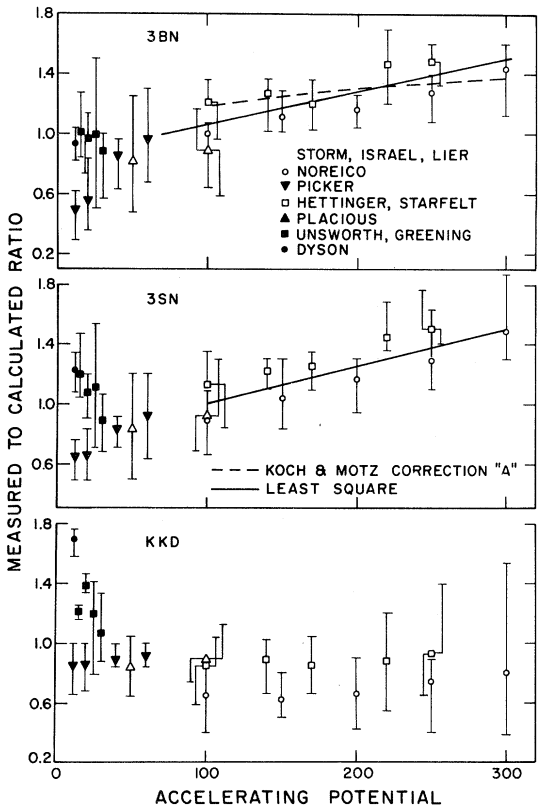

FIG. 11. Measured-to-calculated ratios as a function of accelerating potential.

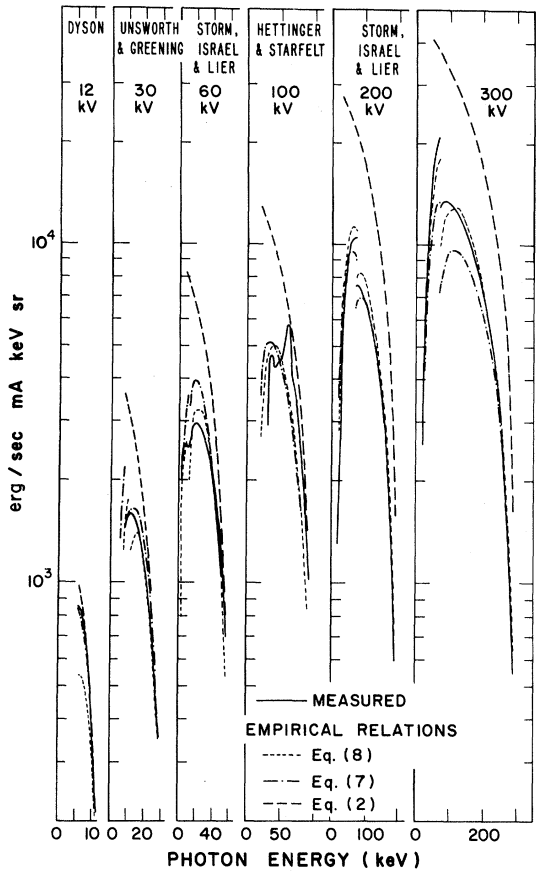

FIG. 12. Comparison of semiempirical equations with measurement. Equation (2) is the KKD formula and Eq. (7) is an approximation to formula 3BN with electron energy losses included, multiplied by backscatter and photon attenuation corrections. Equation (8) is an approximation to formula 3BN with electron energy and backscatter losses included, multiplied by the photon attenuation correction.

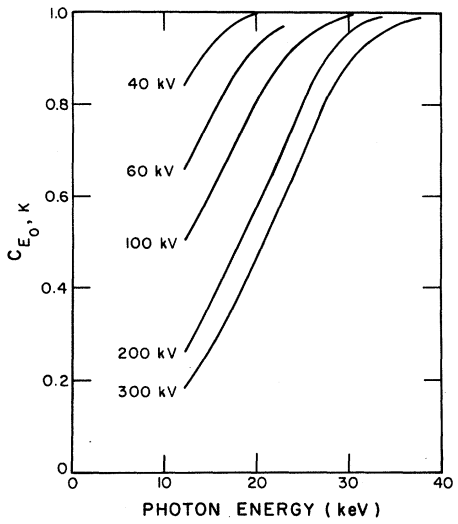

FIG. 13. Factor appearing in the approximate photon attenuation correction [Eq. (9)].

addition, the electron energy loss term dE/dx does not include detours caused by multiple elastic Coulomb scattering by atoms. Because of these approximations and the variations in the measurements, the correctness of the various bremsstrahlung cross sections cannot be determined. Both the thin-target Born approximation formula 3BN, with the Elwert Coulomb correction, and the Sommerfeld formula 3SN give 20% agreement with measurement over the 12–100-keV energy range by considering electron energy and backscatter losses, and photon attenuation. The agreement can be extended to 300 keV by including the Koch and Motz[11] empirical correction.

*Work performed under the auspices of the U. S. Atomic Energy Commission.

[1]M. Ehrlich, J. Res. Natl. Bur. Std. (U.S.) 54, 107 (1955).

[2]M. H. Unsworth and J. R. Greening, Phys. Med. Biol. 15, 621 (1970).

[3]E. Storm, H. I. Israel, and D. W. Lier, Los Alamos Scientific Laboratory Report No. LA-4624, 1971 (unpublished).

[4]G. Hettinger and N. Starfelt, Acta Radiol. 50, 381 (1958).

[5]N. A. Dyson, Proc. Phys. Soc. (London) 73, 924 (1959).

[6]R. C. Placious, J. Appl. Phys. 38, 2030 (1967).

[7]H. A. Kramers, Phil. Mag. 46, 836 (1923).

[8]M. J. Berger and S. M. Seltzer, Natl. Bur. Std. Report Nos. 9836, 9837, 1968 (unpublished).

[9]M. J. Berger and S. M. Seltzer, National Aeronautics and Space Administration Report No. SP-169, 1968, (unpublished), pp. 285–322.

[10]M. J. Berger and S. M. Seltzer, Phys. Rev. C 2, 621 (1970).

[11]H. W. Koch and J. W. Motz, Rev. Mod. Phys. 31, 920 (1959).

[12]A. Sommerfeld, Ann. Physik 11, 257 (1931).

[13]H. Brysk, C. D. Zerby, and S. K. Penny, Phys. Rev. 180, 104 (1969).

[14]G. Elwert and E. Haug, Phys. Rev. 183, 90 (1969).

[15]H. K. Tseng and R. H. Pratt, Phys. Rev. A 3, 100 (1971).

[16]D. H. Rester, N. Edmonson, and Q. Peasley, Phys. Rev. A 2, 2190 (1970).

[17]P. Kirkpatrick and L. Wiedman, Phys. Rev. 67, 321 (1945).

[18]W. Heitler, *Quantum Theory of Radiation* (Oxford U.P., London, 1954), p. 244.

[19]H. Bethe and W. Heitler, Proc. Roy. Soc. (London) A146, 83 (1934).

[20]F. Sauter, Ann. Physik 20, 404 (1934).

[21]R. L. Gluckstern and M. H. Hull, Jr., Phys. Rev. 90, 1030 (1953).

[22]G. Elwert, Ann. Physik 34, 178 (1939).

[23]M. J. Berger and S. M. Seltzer, Natl. Acad. Sci.

Natl. Res. Council Nucl. Sci. Ser. No. 39, 205 (1964).
[24]H. Kulenkampff, Ann. Physik 69, 548 (1922).
[25]H. E. Bishop, *X-Ray Optics and Microanalysis* (Hermann, Paris, 1966), Vol. IV, p. 153.
[26]R. F. J. Heinrich, *X-Ray Optics and Microanalysis* (Hermann, Paris, 1966), Vol. IV, p. 157.
[27]J. O. Brand, Ann. Physik 26, 609 (1936).
[28]W. Bothe, Z. Naturforsch. 4a, 542 (1949).
[29]E. J. Sternglass, Phys. Rev. 95, A345 (1954).
[30]H. Kulenkampff and W. Z. Spyra, Z. Physik 137, 416 (1954).
[31]E. Storm and H. I. Israel, Nucl. Data Tables A7, 565 (1970).
[32]D. H. Rester, W. E. Dance, and J. H. Derrickson, J. Appl. Phys. 41, 2682 (1970).

PHYSICAL REVIEW A VOLUME 5, NUMBER 6 JUNE 1972

Muonium. III. Precision Measurement of the Muonium Hyperfine-Structure Interval at Strong Magnetic Field*

W. E. Cleland,† J. M. Bailey,‡ M. Eckhause,§ V. W. Hughes, R. Prepost,‖ J. E. Rothberg,** and R. M. Mobley††
Gibbs Laboratory, Yale University, New Haven, Connecticut 06520
(Received 28 December 1971)

A complete discussion is given of our precision measurement of the hyperfine-structure interval $\Delta\nu$ of the ground state of muonium at a strong magnetic field of 5000 G. Particular emphasis is placed on refinements to the theory of the resonance line shape and on a detailed discussion of the sources of error and of the capability of our method. The final result for $\Delta\nu$ is $\Delta\nu = 4463.24 \pm 0.12$ MHz (27 ppm), in which the 1-standard-deviation error is caused principally by the statistical counting error and magnetic field inhomogeneity. Allowance is included for a quadratic as well as a linear dependence of $\Delta\nu$ on pressure. This result is in good agreement with other, more precise, experimental values and with the current theoretical value $\Delta\nu = 4463.326 \pm 0.019$ MHz (4.2 ppm).

I. INTRODUCTION

This paper gives a detailed discussion of our precision measurement of the hyperfine-structure interval $\Delta\nu$ of muonium through the observation of a magnetic resonance transition at strong magnetic field. The motivation for a precise determination of $\Delta\nu$ and the general theory and experimental method of magnetic resonance studies of muonium have been discussed[1,2] in Paper II of this series. The present paper emphasizes a detailed discussion of errors in this experiment.

Section II presents a discussion of refinements in the theory of the resonance line shape, as compared to the simpler discussion[1] in Paper II. Section III describes the experimental method and apparatus, in particular, the new features relevant to a high-precision experiment. Section IV presents the data analysis, which includes a detailed consideration of errors and of the hfs pressure or density shift. Finally, Sec. V gives our results and conclusions. Brief reports of this research have been published.[2-4]

II. REFINEMENTS IN THEORY OF RESONANCE LINE SHAPE

Refinements to the theory of the resonance line shape as given in Paper II[1] must be considered for the higher-precision measurement reported in the present paper. The effects of the following factors, which were neglected in the derivation of the resonance line shape of Eq. (2.28) of Paper II [II 2.28] will be treated:

(1) Muonium states other than the two directly involved in the resonance transition.

(2) Formation of both muonium states involved in the resonance transition as the initial condition for the transition process.

(3) Off-resonance frequency component $e^{+i\omega t}$ (or $e^{-i\omega t}$) in the microwave magnetic field.

(4) Inhomogeneity of the static magnetic field $\vec{H}$.

(5) Spatial variation of the applied microwave magnetic field $\vec{H}_1$. Also a component of $\vec{H}_1$ parallel to $\vec{H}$.

(6) Finite time interval of observation of the transition process.

(7) Spatial distribution of the stopped muons.

(8) Dependence of the decay positron asymmetry on the positron energy.

(9) The solid angle subtended by the positron detectors.

(10) Trajectories of the decay positrons in the static magnetic field $\vec{H}$.

In order to treat these refinements to the resonance line shape and to develop a more general formula for the line shape, it is best to start again from the beginning. For the present we still assume that only two muonium states, designated 1 and 2 with energies W_1 and W_2, are involved. The